



Iron-spin transition controls structure and stability of LLSVPs in the lower mantle



Chuan Huang^{a,b}, Wei Leng^{a,b,*}, Zhongqing Wu^{a,b}

^a Laboratory of Seismology and Physics of Earth's Interior, School of Earth and Space Sciences, University of Science and Technology of China, Hefei 230026, China

^b National Geophysical Observatory at Mengcheng, Anhui, China

ARTICLE INFO

Article history:

Received 9 February 2015

Received in revised form 3 May 2015

Accepted 4 May 2015

Available online 15 May 2015

Editor: B. Buffett

Keywords:

LLSVPs

lower mantle

spin transition

ferropericlasite

ABSTRACT

Seismic tomography models have revealed that there exist two large low shear velocity provinces (LLSVPs) beneath Africa and the Pacific Ocean in the Earth's lower mantle. Waveform modeling results suggest both LLSVPs have steep sharp side boundaries, which imply that they probably are compositionally heterogeneous from the ambient mantle. When applying the surface plate motion history in the last a few hundred million years (Ma) as the driving mechanism, numerical modeling has successfully reproduced the geographical distribution of the two LLSVPs in thermochemical mantle convection. However, two prominent seismic features of the LLSVPs, the steep side boundaries and the high elevation, can hardly be obtained in previous geodynamic models. Here, we include in our mantle convection model the effects of iron-spin transition of ferropericlasite which substantially change physical properties of the mantle. Our results show that iron-spin transition plays a dominant role in controlling the structure and stability of LLSVPs. Large chemical blocks with steep side boundaries and high elevations up to ~1200 km above core–mantle boundary (CMB) emerge in our models with the volume content of ferropericlasite ~20%. Such blocks cause a shear wave velocity decrease of ~3.5% which is consistent with the seismic observations. Our results also show that these LLSVPs are transient structures in the lower mantle, which can typically last for a few hundred million years before destroyed by large-scale mantle motion.

© 2015 Elsevier B.V. All rights reserved.

1. Introduction

Two large low shear velocity provinces (LLSVPs) in the Earth's lower mantle have been identified from seismic tomography studies for their rapidly decreased shear wave velocity compared with the ambient mantle (Grand et al., 1997; Ritsema et al., 1999). The two LLSVPs are located nearly antipodal beneath Africa and the central Pacific Ocean, both with high elevations and steep side boundaries based on seismic waveform modeling studies (Ni et al., 2002; Ni and Helmberger, 2003; He and Wen, 2009). The African one extends 1200–1500 km upward from the core–mantle boundary (CMB) with steep and sharp side boundaries (Ni et al., 2002; Wang and Wen, 2007). The structure of LLSVP beneath the Pacific Ocean is less clear. It has been suggested that there exist two separated parts with ~700 km and ~300 km in height respectively (He and Wen, 2009). Similar to the Africa block, both Pacific parts

have steep and sharp side boundaries (He and Wen, 2009). Besides the decreased shear wave velocity, the two LLSVPs also show anti-correlations between shear velocity and bulk sound velocity near the CMB (Ishii and Tromp, 2004). These seismic observations together suggest a chemical origin for the LLSVPs, possibly from the accumulation of recycled slabs or from the remnant material of dense melt formed in early evolution history of the Earth (Christensen and Hofmann, 1994; Labrosse et al., 2007).

Studying the formation and stability of these two LLSVPs is one of the key issues in understanding the evolutionary history of the Earth's lower mantle. Thermochemical geodynamic modeling has been employed to investigate the evolution of the two LLSVPs in large-scale mantle convection (McNamara and Zhong, 2005; Zhang et al., 2010; Tan et al., 2011). With the imposed plate motion history in the last 120 million years (Ma) as the surface boundary condition, McNamara and Zhong (2005) successfully reproduced the antipodal geographical distribution of the two LLSVPs beneath Africa and the Pacific Ocean. However, it is rather subtle to produce a chemical block with structures similar to the seismic observations, i.e. structures with high elevations and steep side boundaries. The structure of the LLSVPs is sensitive to their chemical density contrast compared with the

* Corresponding author at: Laboratory of Seismology and Physics of Earth's Interior, School of Earth and Space Sciences, University of Science and Technology of China, Hefei 230026, China.

E-mail address: wleng@ustc.edu.cn (W. Leng).

ambient mantle (Ni et al., 2002; McNamara and Zhong, 2005; Tan and Gurnis, 2007). A small density contrast leads to quick mixture of the chemical composition with the ambient mantle. On the other hand, a large density contrast forms a flat layer without large topography at the base of the mantle (e.g. Tan and Gurnis, 2007). One possible way to form a stable chemical structure with high elevation and steep side boundaries is by assigning a different compressibility for the chemical composition compared with the ambient mantle (Tan and Gurnis, 2005). This setting leads to two distinct density profiles for the chemical material and the ambient mantle. The elevation of the chemical block is then controlled by a “height of neutral buoyancy” where two density profiles intersect each other (Tan and Gurnis, 2005, 2007). However, how to determine the neutral buoyancy height remains a difficult question.

The geographical stability of the two LLSVPs is another issue under great debate. Based on the reconstruction of large igneous provinces (LIPs), some studies propose that these two LLSVPs have been geographically stable since 300 Ma (Torsvik et al., 2008) or existed even much longer as an old isolated reservoir (Burke et al., 2008). But geodynamic modeling results indicate that these two LLSVPs may be transient structures which can only last for several hundred million years in large-scale mantle convection (Zhang et al., 2010; Tan et al., 2011).

In previous thermochemical mantle convection models, they did not consider an electronic reconfiguration of iron under temperature–pressure conditions of the lower mantle: spin transition. Spin transition of iron has been observed in both ferropericlase [(Mg,Fe)O] and bridgmanite (Tschauner et al., 2014) [(Mg,Fe)(Si,Al,Fe)O₃] which volumetrically take up ~17% and ~79% of the lower mantle, respectively (Badro et al., 2003; Lin et al., 2013). Iron in bridgmanite is more complex than iron in Fp: it can exist in Fe²⁺ and Fe³⁺ states and can occupy the A site and B site. First-principles calculations show that the extremely high quadruple splitting value of Fe²⁺ in bridgmanite above ~30 GPa, which has been interpreted as the high-spin to the intermediate-spin transition (Lin et al., 2008; McCammon et al., 2008), results from the change of local structure of A site Fe²⁺ (Bengtson et al., 2009; Hsu et al., 2011), whose effect on density and bulk modulus are much smaller than the effect of spin transition on density and bulk modulus of ferropericlase (Lundin et al., 2008). The experimental and theoretical studies show that only B site Fe³⁺ experiences high spin to low spin transition at lower mantle pressure (Stackhouse et al., 2007; Hsu et al., 2011; Fujino et al., 2012). The abundance of B site Fe³⁺, however, is still under debate. Some experiments show that (B site Fe³⁺)/(total Fe) is negligible at lower mantle pressure (e.g. Glazyrin et al., 2014). For this reason, we only focus on the effects of iron-spin transition in ferropericlase.

When the transition in ferropericlase occurs, the number of unpaired *d* electrons of Fe²⁺ decreases from four to zero, leading to the reduction of volume of iron atom, which significantly changes the physical properties of ferropericlase (e.g. Lin et al., 2013). The spin transition of iron causes anomalous softening of the bulk modulus of ferropericlase (Marquardt et al., 2009; Wentzcovitch et al., 2009; Wu et al., 2013) which produces an unusual effect: P wave of pyrolitic lower mantle becomes temperature insensitive at the depth of ~1750 km (Wu and Wentzcovitch, 2014). This effect provides reasonable explanations to most of the unusual results disclosed by seismic tomography at middle lower mantle such as the disruption of P wave image below some hot spots (Zhao, 2007) and the global disruption of P wave structure (van der Hilst and Kárason, 1999), which suggest that spin transition of iron in ferropericlase indeed occurs at lower mantle, although the spin transition is not visible in one-dimensional seismic velocity profile (Masters, 2008). The anomalous thermodynamics properties of ferropericlase caused by spin transition (Wu

et al., 2009) inspire investigations of their effects on mantle convection. It has been shown that iron-spin transition enhances the vigor of plumes in numerical simulations of purely thermal mantle convection (Bower et al., 2009; Shahnas et al., 2011). However, the influence of iron-spin transition on thermochemical convection has not been discussed yet.

The purpose of this work is to investigate the influence of the iron-spin transition of ferropericlase on thermochemical mantle convection, particularly on the formation and stability of LLSVPs in the lower mantle. We first provide the governing equations and parameterization of iron-spin transition in our model. Then we show that iron-spin transition may significantly influence the structure and stability of LLSVPs.

2. Methods

We construct our model in a spherically axisymmetric geometry with a modified extended Boussinesq approximation (King et al., 2010). The non-dimensional conservation equations of mass, momentum and energy for thermochemical convection are as below,

$$\nabla \cdot \mathbf{u} = 0, \quad (1)$$

$$-\nabla p + \nabla \cdot [\eta(\nabla \mathbf{u} + \nabla \mathbf{u}^T)] - [Ra\rho\alpha(T - T_r) - Ra_c C] \mathbf{g} = 0, \quad (2)$$

$$\frac{DT}{Dt} - Di\alpha\mathbf{g}\mathbf{u}(T + T_s) = \nabla \cdot (\kappa\nabla T) + \frac{Di}{Ra}\Phi + H. \quad (3)$$

Here, the variables are the velocity vector \mathbf{u} , dynamic pressure p , viscosity η , density ρ , thermal expansivity α , temperature T , horizontally averaged temperature T_r , chemical composition C (varying between 0 and 1), gravitational acceleration vector \mathbf{g} , surface temperature T_s , thermal diffusivity κ , viscous diffusivity Φ and heat production rate H . Each of these variables is non-dimensional. Rayleigh number Ra and chemical Rayleigh number Ra_c in Eq. (2) are defined as:

$$Ra = \frac{\rho_0\alpha_0g_0\Delta TR^3}{\kappa_0\eta_0}, \quad (4)$$

$$Ra_c = Ra \frac{\Delta\rho'_c}{\rho_0\alpha_0\Delta T}, \quad (5)$$

where ρ_0 is surface density; α_0 is surface thermal expansivity; g_0 is surface gravitational acceleration; ΔT is temperature contrast between surface and CMB; R is radius of the Earth; κ_0 is surface thermal diffusivity; η_0 is reference viscosity and $\Delta\rho'_c$ is chemical density anomaly. They are all dimensional variables. The physical constants used in our models can be found in Table 1. In all of our models, Ra is fixed at 10^8 (except for Cases 14–20, see Table S1 in supplementary materials), corresponding to a reference lower mantle viscosity of $\sim 9 \times 10^{21}$ Pa.s. Di is the dissipation number which can be expressed as:

$$Di = \frac{\alpha_0g_0R}{C_{p,0}}, \quad (6)$$

where $C_{p,0}$ is the dimensional surface specific heat (Table 1).

We add a depth-dependent density profile in the buoyancy term. The non-dimensional density profile can be expressed as

$$\rho(z) = \exp(\chi z). \quad (7)$$

Here, χ is the mantle compressibility and z is the non-dimensional depth normalized by the Earth's radius (Table 1). The parameters used lead to a factor of ~1.65 increase in density from surface to CMB, similar to the Earth's mantle density distribution.

Table 1
Physical parameters and constant variables.

Parameters	Value
Earth radius R	6371 km
Mantle thickness d	2870 km
Surface thermal expansivity α_0	$3 \times 10^{-5} / \text{K}$
Surface thermal diffusivity κ_0	$1 \times 10^{-6} \text{ m}^2/\text{s}$
Surface density ρ_0	3400 kg/m^3
Surface specific heat $C_{p,0}$	1200 $\text{J}/(\text{kgK})$
Surface gravitational acceleration g_0	10.0 m/s^2
Mantle compressibility χ	1.11
Dissipation number D_i	1.6
Surface temperature $T_{s,0}$	273 K
Temperature contrast between surface and bottom ΔT	3500 K

From surface to CMB, the thermal expansivity α decreases linearly by a factor of 2.0 and the thermal diffusivity κ increases linearly by a factor of 2.18. The thermal expansivity is a parameter affecting the stability of mantle plumes (Hansen and Yuen, 2000). We will later discuss the effect of different depth-dependent profiles of thermal expansivity on our results.

The viscosity used in our model is dependent on both depth and temperature. The non-dimensional form of viscosity can be expressed as:

$$\eta(T, z) = \eta_r(z) \exp[A(0.5 - T)]. \quad (8)$$

Here, $\eta_r(z)$ is 1/30 in upper mantle except for lithosphere (depth <100 km) where $\eta_r(z)$ is 1/3; For the lower mantle, $\eta_r(z) = 1$. This formulation gives us a weaker upper mantle and a viscous jump of 30 times at the upper–lower mantle boundary. The activation energy A is set to 6.908, leading to a viscous drop of 1000 times when non-dimensional temperature changes from 0.0 to 1.0.

In our model, the effects of the iron-spin transition are considered only in the buoyancy term. The dimensional density variation in mantle convection model can be expressed as (modified after Jarvis and Mckenzie, 1980):

$$\Delta \rho' = \rho'(-\alpha' \Delta T' + p'/K_T') + \Delta \rho'_c, \quad (9)$$

where ρ' and α' are depth-dependent density and thermal expansivity respectively. $\Delta T'$ is temperature perturbation; p' is dynamic pressure; K_T' is isothermal bulk modulus. When iron-spin transition occurs, the new $\Delta \rho'$ can be written in the form that is similar to Shahnas et al. (2011):

$$\Delta \rho' = \rho'(-\alpha' \Delta T' + p'/K_T') + \Delta \rho'_{spin} + \Delta \rho'_c. \quad (10)$$

Here, $\Delta \rho'_{spin}$ is the total density change due to spin transition, it contains three parts:

$$\Delta \rho'_{spin} = \Delta \rho'_{s_rho} + \Delta \rho'_{s_alpha} + \Delta \rho'_{s_bulk}, \quad (11)$$

where $\Delta \rho'_{s_rho}$ is the density change directly due to iron-spin transition (we further denote it as $\Delta \rho'_s$); $\Delta \rho'_{s_alpha}$ and $\Delta \rho'_{s_bulk}$ are also density changes, but they are relate to the variations of thermal expansivity and bulk modulus respectively, i.e.

$$\Delta \rho'_{s_alpha} = -\rho' \Delta \alpha'_s \Delta T', \quad (12)$$

$$\Delta \rho'_{s_bulk} = \rho' \left(\frac{p'}{K_T' + \Delta K'_s} - \frac{p'}{K_T'} \right), \quad (13)$$

where $\Delta \alpha'_s$ and $\Delta K'_s$ are the variations in thermal expansivity and bulk modulus (we assume it is isothermal bulk modulus) caused by iron-spin transition. We need to note that parameters $\Delta \rho'_s$, $\Delta \alpha'_s$ and $\Delta K'_s$ are the physical property changes for the whole lower mantle. If we assume ferropericlasite takes up 20% of the lower

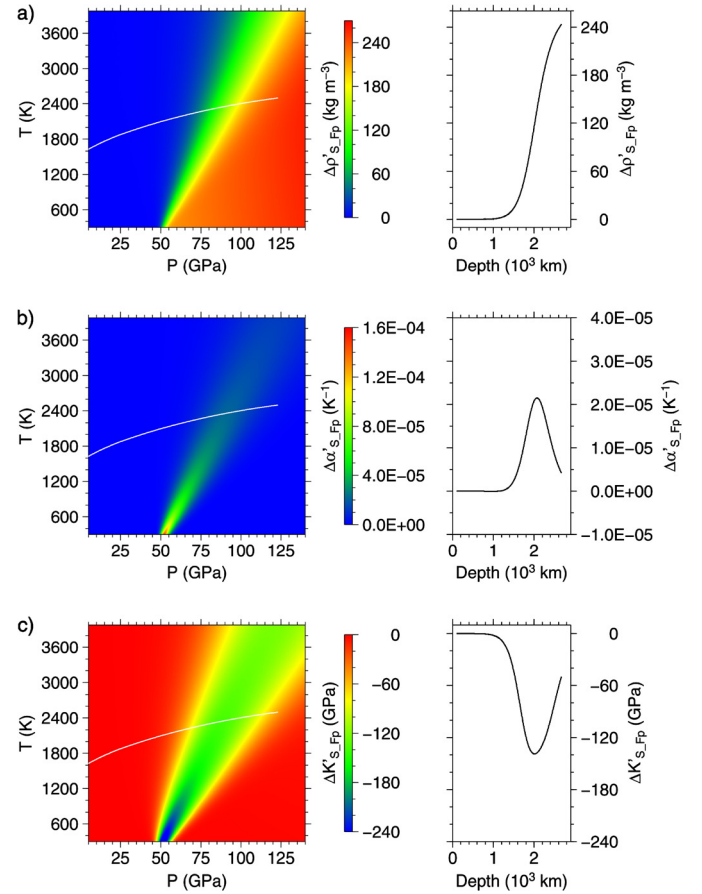


Fig. 1. Spin-induced property anomalies of ferropericlasite ($\text{Mg}_{1-x}\text{Fe}_x\text{O}$ where $x = 0.1875$) relative to temperature and pressure. (a), (b) and (c) are variations of density, thermal expansivity and bulk modulus, respectively. The white lines in left column of (a)–(c) are a typical geothermal profile. The corresponding values along the profile are plotted in the right column of (a)–(c).

mantle by volume, then the relations between the mantle and ferropericlasite for these three properties can be easily obtained from relations of Maxwell (Poirier, 2000) in the following format:

$$\Delta \rho'_s = \frac{1}{5} \Delta \rho'_{s_Fp} \quad (14)$$

$$\Delta \alpha'_s = \frac{1}{5} \Delta \alpha'_{s_Fp} \quad (15)$$

$$\frac{1}{K_T' + \Delta K'_s} - \frac{1}{K_T'} = \frac{1}{5} \left(\frac{1}{K_T' + \Delta K'_{s_Fp}} - \frac{1}{K_T'} \right) \quad (16)$$

where $\Delta \rho'_{s_Fp}$, $\Delta \alpha'_{s_Fp}$ and $\Delta K'_{s_Fp}$ are the spin-induced variations of density, thermal expansivity and bulk modulus for ferropericlasite, respectively. These three values change dramatically with pressure and temperature at spin crossover region based on the first-principles calculation (Fig. 1) (Wu et al., 2009). We will later discuss the effect of different volume content of ferropericlasite on our results.

We use a modified version of 2-D finite element code, Citcom, (Moresi and Solomatov, 1995) to perform the numerical simulations in the spherically axisymmetric geometry. The calculation of $\Delta \rho'_{spin}$ is included in the modified program. At each time step, the program searches the values of $\Delta \rho'_{s_Fp}$, $\Delta \alpha'_{s_Fp}$, $\Delta K'_{s_Fp}$ from Fig. 1 based on the temperature and pressure at each node, then adds them to $\Delta \rho'$ as described in Eq. (10). The grid resolution is 385 by 129 nodes in θ and r directions respectively, where θ is from 0° to 90° and r is from CMB to surface. $\theta = 0^\circ$ corresponds to the north pole. The left and right boundaries are reflective. The surface and

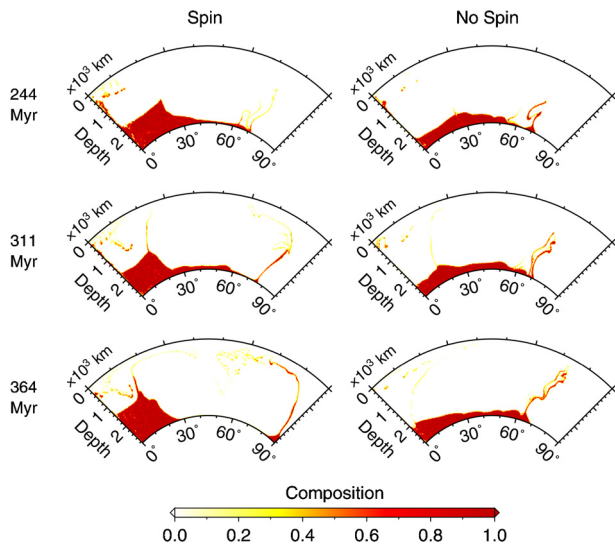


Fig. 2. Compositional fields of Case 1 (left column) and Case 2 (right column) at 244, 311 and 364 Myr of evolutionary history, respectively. The left boundary is aligned with the pole and the volume of chemical material in the plot needs to be scaled with $2\pi r \sin \theta$ (r and θ are respectively the radius and co-latitude of an element).

bottom boundaries are free-slip with fixed non-dimensional temperature at 0 and 1, respectively. Our models are initiated with a temperature field which is obtained by running the purely thermal convection to a statistically steady state. A flat chemical layer of 200 km thick is then added above the CMB as the starting point. Chemical composition is tracked with the tracer ratio method (e.g. Tackley and King, 2003) and each element initially contains 16 tracers. We will later discuss the effect of different initial thickness of the chemical layer on our results.

We also calculate the perturbation of shear wave velocity in our model by using the method provided by Deschamps and Trampert (2003), in which the lateral heterogeneity of velocity is induced by the variations in temperature and composition. The variation in composition can further be simplified as the chemical density anomaly in our model (assuming this anomaly is totally due to the change of iron content in bridgmanite). Note that this method only works well for the mixture of bridgmanite and ferropericlase. Therefore we only compute the velocity perturbation in the lower mantle.

3. Results

Fig. 1 shows the change of density, thermal expansivity and bulk modulus induced by iron-spin transition of ferropericlase. These data are modified from the results of Wu et al. (2009) with a constant shift in Gibbs free energy of high spin state of ferropericlase, which moves the spin-transition pressure to the experimental result at room temperature (Wu and Wentzcovitch, 2014). Different from a phase transition, the iron-spin transition is a process of gradual change (Fig. 1). For a typical geothermal profile, the transition starts from the depth of ~ 1400 km and becomes noticeable at the depth of ~ 1700 km.

Case 1 is a representative model which shows the influence of iron-spin transition on thermochemical mantle convection (Table S1). It starts with a 200 km chemical layer which is 2.2% denser than the surrounding mantle and the thermal expansivity decreases by a factor of 2 from surface to the CMB (Table S1). The left column of Fig. 2 shows the compositional fields of Case 1 at three snapshots of different time. It can be observed that the transition in spin state has significant effect on shaping the structure of chemical piles in the lower mantle. With the influence of spin transition, chemical layer forms a huge block at the left mar-

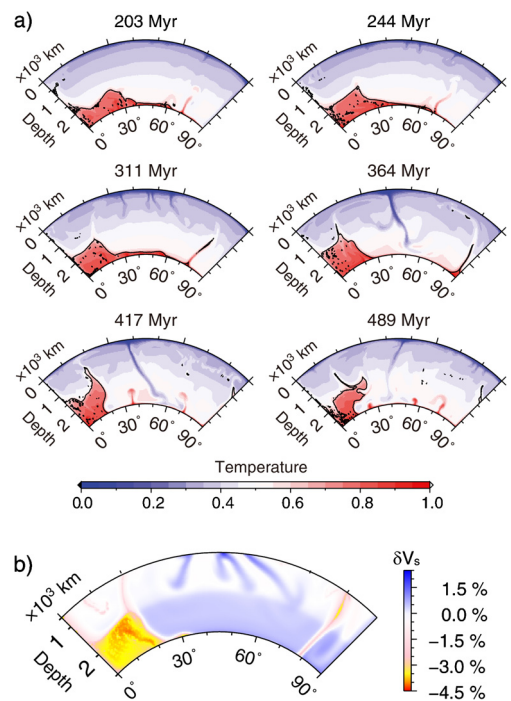


Fig. 3. (a) Non-dimensional temperature fields (the value 0 and 1 correspond to 273 and 3773 K, respectively) of Case 1 at 203, 244, 311, 364, 417, 489 Myr. The black lines in plots are contour lines where $C = 0.8$ (it also applies to Figs. 6–9). (b) Calculated shear velocity perturbations in the lower mantle for Case 1 at 311 Myr.

gin of the model with steep side boundaries and high elevation to ~ 1200 km above CMB. These features make the block quite similar to the LLSVP beneath Africa in morphology (Ni et al., 2002). Case 2 is identical to Case 1 except that it ignores the influence of iron-spin transition. The evolutionary results of Case 2 are shown in the right column of Fig. 2. In this case, the chemical layer just forms a flat and broad layer at the bottom of the mantle.

We estimate the formation and destruction time of the chemical blocks with an empirical way: when the size of a chemical block reaches more than 700 km in both r and θ directions, and the slope angle of the side boundary is larger than 50° , we take the time as the formation time; when the chemical block is significantly altered by the large-scale mantle convection (usually by cold downwellings) to lose its block shape, we take the time as the destruction time. The time interval between the formation and destruction time is defined as the lifespan of a chemical block. The huge chemical block structure in Case 1 forms at ~ 203 million year (Myr) and survives for ~ 300 million years. After ~ 489 Myr, the structure begins to be destroyed by large-scale mantle motion (Fig. 3a). The survival period of this huge chemical block can be divided into 3 stages: formation (203 and 244 Myr in Fig. 3a), stable (311 and 364 Myr in Fig. 3a) and destruction (417 and 489 Myr in Fig. 3a). Two major factors contribute to the destroying of the chemical structure: the entrainment of chemical material by large-scale upwellings and the strong push from downwelling slabs right above the chemical pile.

The corresponding variations of shear velocity in the lower mantle for Case 1 at 311 Myr are presented in Fig. 3b. The calculated shear velocities decrease by 3%–4% in the chemical block, which is consistent with seismic observations (Wang and Wen, 2007; He and Wen, 2009).

We then extract each part of density perturbation $\Delta\rho'_{spin}$ in Case 1 at 311 Myr, including $\Delta\rho'_{s_rho}$, $\Delta\rho'_{s_alpha}$ and $\Delta\rho'_{s_bulk}$, and present them in Fig. 4a–c. It can be observed that in the lower mantle, $\Delta\rho'_{s_rho}$ and $\Delta\rho'_{s_alpha}$ are smaller in the chemical

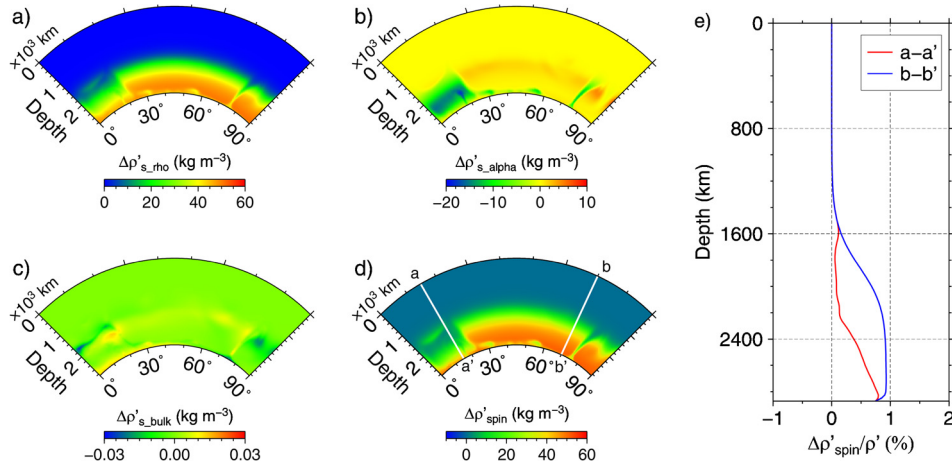


Fig. 4. The distributions of (a) $\Delta\rho'_{s_rho}$, (b) $\Delta\rho'_{s_alpha}$, (c) $\Delta\rho'_{s_bulk}$ and their total value (d) $\Delta\rho'_{spin}$ for Case 1 at 311 Myr. (e) denotes the depth profiles of percentage of $\Delta\rho'_{spin}$ relative to ρ' on white lines a–a' and b–b' drawn in (d) (red line for a–a', blue line for b–b'). (For interpretation of the references to color in this figure legend, the reader is referred to the web version of this article.)

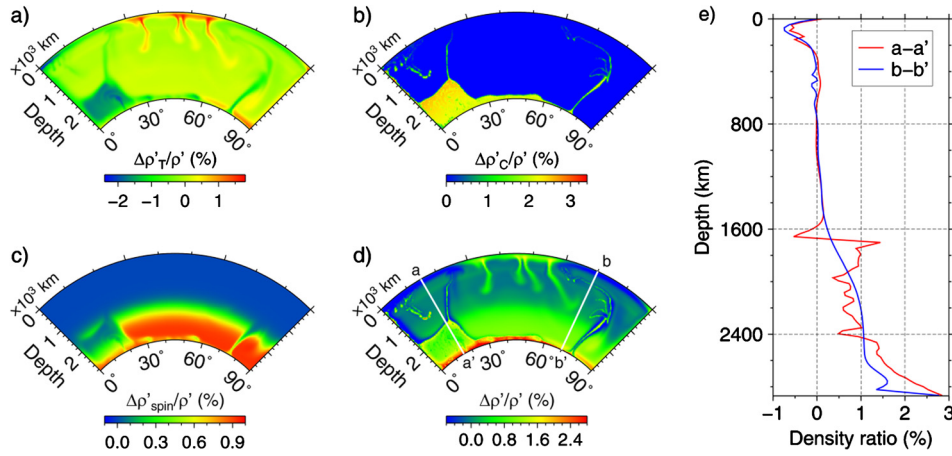


Fig. 5. Density perturbations due to (a) temperature, (b) composition and (c) spin transition for Case 1 at 311 Myr, respectively. The summations of (a), (b) and (c) are showed in (d). (e) denotes the depth profiles of perturbation of $\Delta\rho'$ relative to ρ' on white lines a–a' and b–b' drawn in (d) (red line for a–a', blue line for b–b'). (For interpretation of the references to color in this figure legend, the reader is referred to the web version of this article.)

block which has a higher temperature. Compared with $\Delta\rho'_{s_rho}$ and $\Delta\rho'_{s_alpha}$, $\Delta\rho'_{s_bulk}$ is negligible in magnitude because the dynamic pressure is only $\sim 1/1000$ of bulk modulus. The density contrast between the chemical block region and the ambient mantle induced by the iron-spin transition appears at the depth of ~ 1400 km and is $\sim 0.3\%$ at the depth of 1700 km (Fig. 4d–e). Between 1700 km depth and CMB, the density contrast first increases to $\sim 1\%$ then decreases to 0 (Fig. 4d–e). Such a density contrast is the critical factor in promoting the formation of huge chemical blocks with steep side boundaries and high elevations. The LLSVP beneath Africa rise to ~ 1700 km depth, which is consistent with the depth in our numerical model where the iron-spin transition causes significant density contrasts between the chemical block region and the ambient mantle (Fig. 4d–e).

The density perturbation shown in Eq. (10) is caused by three factors: temperature, composition and iron-spin transition. We denote the corresponding density variations due to these three factors as $\Delta\rho'_T$, $\Delta\rho'_C$ and $\Delta\rho'_{spin}$ respectively. Their percentages relative to reference density ρ' for Case 1 at 311 Myr are shown in Fig. 5. It can be observed that the total density perturbation in the chemical block region ($\Delta\rho'_T + \Delta\rho'_C + \Delta\rho'_{spin}$) nearly equals to the density perturbation in the ambient mantle. The density balance between the chemical block and the ambient mantle keeps

the chemical structure stable until it is destroyed by large scale mantle motion, such as strong upwellings or downwellings.

The formation of the meta-stable chemical block is sensitive to its intrinsic chemical density contrast. We test the effect of this contrast by defining $\gamma = \Delta\rho'_C/\rho'_i$, where ρ'_i is the reference density at the upper boundary of the chemical layer at the initial time. We run a series of cases in which γ increases from 1.0% to 3.5% with a step of 0.1%. The typical models with their results are presented in Table S1 (Case 1, and Cases 3–7) and Fig. 6. We can note that, when γ is small (1.0% for Case 3), chemical composition quickly mixes with surroundings; for intermediate γ values (2.0%, 2.2%, 2.4% and 2.6% for Cases 4, 1 and 5–6), huge chemical blocks emerge with a survival time of 200 \sim 300 Myr; when γ becomes too large (3.5% for Case 7), chemical material evolves as a nearly flat layer without large topography above the CMB.

The thickness of initial chemical layer (C_H) and the decreasing factor of thermal expansivity from surface to the CMB (α_{factor}) are two other important parameters which may affect the formation of huge chemical blocks. In Cases 8–10 (Table S1), all the parameters are the same as Case 1 except for C_H and α_{factor} . When C_H changes from 200 km to 300 km (Fig. 7, Case 8), the shape of chemical structure does not change much except that it gets a larger dimension in θ direction. We then test the effect of α_{factor} from 3.0 to 5.0. We find that if $\alpha_{factor} = 3.0$, large chemical blocks can still emerge (Fig. 7, Case 9), but the range of valid γ changes

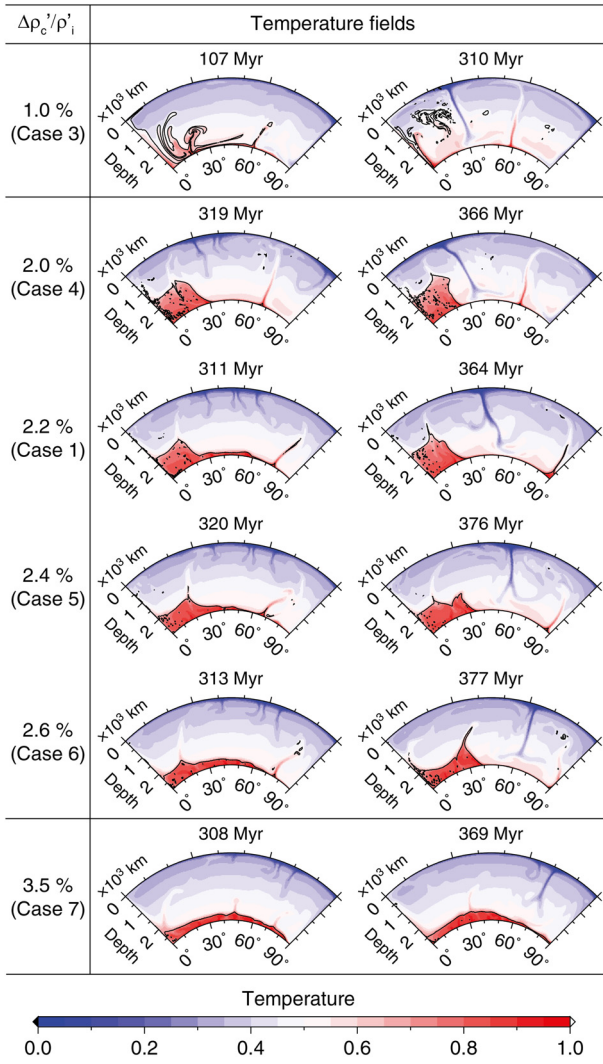


Fig. 6. Evolutionary fields of temperature for Cases 1 and 3–7. Parameters for Cases 3–7 are identical to Case 1 except for their different intrinsic chemical density contrasts.

from 2.0–2.6% to 2.0–2.2%. Once α_{factor} is larger than 4.0, which is far larger than α_{factor} of MgO and MgSiO₃ (~2) (Wentcovitch et al., 2010), the chemical block structures with high elevations and steep side boundaries cannot form any more.

All the above cases assumed that the volume content of ferropericlasite in the chemical layer (C_{FP}) is the same as in the ambient mantle (i.e. 20%), but this assumption may not be appropriate due to the compositional change in the chemical layer. Therefore it is necessary to investigate whether the variable content of ferropericlasite in the chemical layer can significantly influence our results. Based on Case 1, we run several cases by changing C_{FP} from 0.0% to 40.0% with a step of 5.0%. The results show that when C_{FP} equals to 15.0%, 25.0%, and 30.0% the expected chemical block structures still form (Cases 11–13 in Table S1, Fig. 8), verifying the robustness of our results.

Thus far, all these cases ignored the term of internal heating for simplification (i.e. H in Eq. (3) equals to 0.0). To make the model more realistic, we construct a group of new cases in which internal heating contributes to ~60% of the total heating of the mantle (Zhong, 2006; Leng and Zhong, 2008). The import of internal heating increases the average temperature of the mantle, leading to the decrease of viscosity and the increase of average velocity of convection. So we decrease the Rayleigh number from 1e8 to 2e7 to make the new viscosity profile and root-mean-square velocity

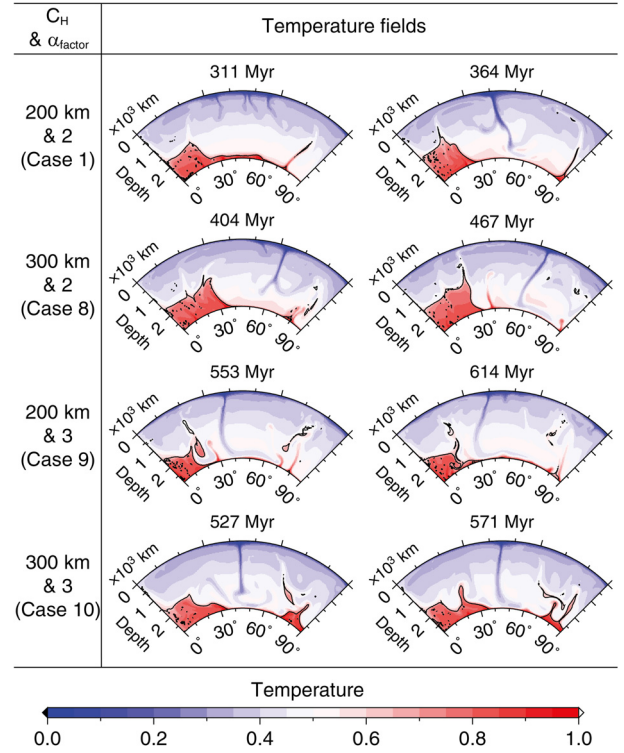


Fig. 7. Evolutionary fields of temperature for Case 1 and Cases 8–10. We use Case 1 as the reference model and then adjust initial chemical layer thickness to 300 km (Case 8) or increase the decreasing factor of thermal expansivity to 3 (Case 9), or both (Case 10).

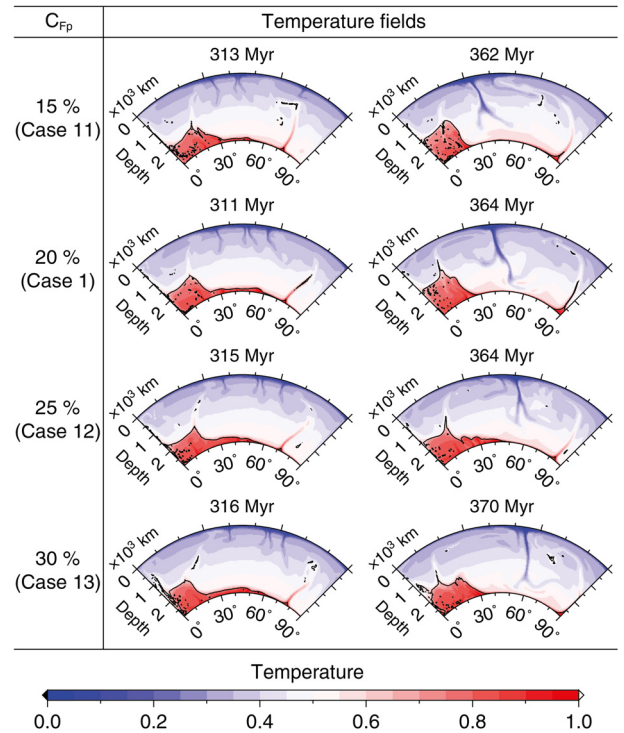


Fig. 8. Evolutionary fields of temperature for Case 1 and Cases 11–13. These cases are the same as Case 1 except for their different volume content of ferropericlasite in the chemical material.

of the mantle comparable to the previous cases. The increased average temperature of the mantle also changes the density contrast of $\Delta\rho'_{spin}$ between the hot chemical block and surroundings. We present the typical results of internal heating cases in Fig. 9

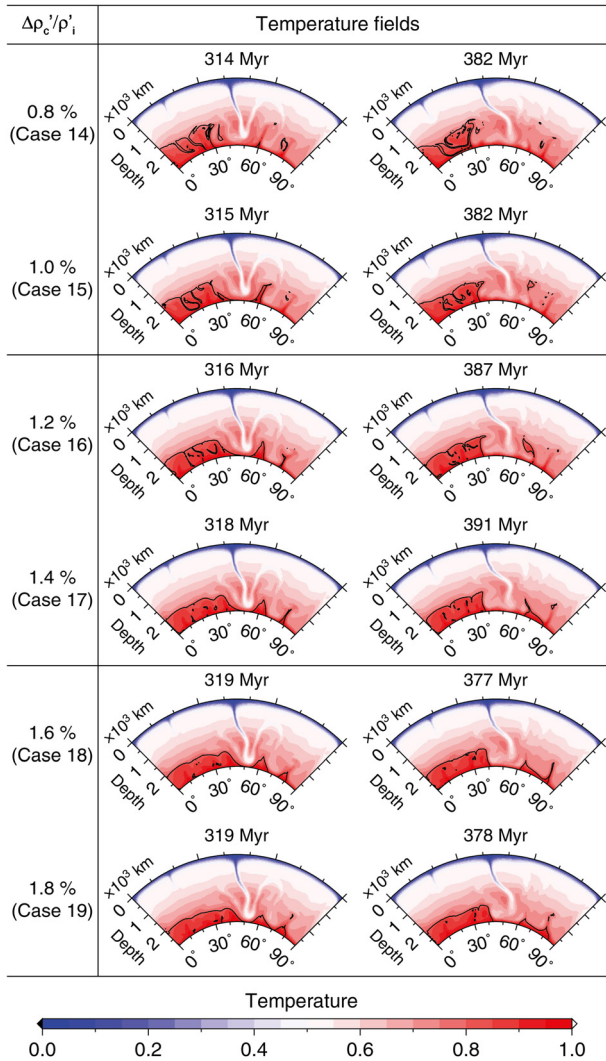


Fig. 9. Evolutionary fields of temperature for Cases 14–19 which considered the effects of internal heating. The initial temperature field is obtained by running the purely thermal convection with internal heating which takes up $\sim 60\%$ of the total heating to a statistically steady state. The Rayleigh number for these cases is adjusted to 2×10^7 .

(Cases 14–19 in Table S1). It can be observed that the effect of internal heating does not significantly influence the shape and the survival time of the chemical block structures. However, the proper range of γ for generating large chemical blocks changes to be 0.8–1.8%. We also find an interesting point for the internal heating cases: The average height of the chemical block (A_H) is related to the value of γ . When γ equals to 0.8 and 1.0, A_H is larger than 950 km (Cases 14, 15); when γ equals to 1.2 and 1.4, A_H is ~ 850 km (Cases 16, 17); and when γ equals to 1.6 and 1.8, A_H is ~ 700 km (Cases 18, 19). These results suggest that with the internal heating effect, the height of the chemical blocks is dependent on their intrinsic chemical density contrast (which is not obvious in previous density ratio tests, i.e. Cases 1 and 3–7).

For all the above cases, the chemical blocks with steep side boundaries and high elevations, once formed, typically survive for 200–300 Myr, no matter how we change the model parameters (i.e. α_{factor} , C_H , C_{Fp} , H). It suggests that the LLSVPs are probably transient structures in the lower mantle which can emerge and disappear as large scale mantle motion evolves.

Finally, we construct an additional model case (Case 20, Table S1) which is identical to Case 1 except that its Rayleigh number is 10^7 , corresponding to a 10 times larger mantle reference viscosity (i.e. $\sim 9 \times 10^{22}$ Pas). The formation and destruction processes

of the chemical block for this case are similar to Case 1 (see supplementary materials for the animation of Case 20). Note that the survival time becomes longer due to the increased mantle viscosity), showing that our results are not sensitive to a larger mantle viscosity.

4. Discussions and conclusions

The density contrast of $\Delta\rho'_{spin}$ between the chemical block and the ambient mantle (Fig. 4d, e) is the key point in promoting the formation of large chemical blocks with steep side boundaries and high elevations. When the iron-spin transition is not included, the chemical layer is either entirely entrained by the upwelling plumes (for a small intrinsic chemical density contrast) or remains a nearly flat layer (for a large intrinsic chemical density contrast). But when the iron-spin transition is included, $\Delta\rho'_{spin}$ is smaller in the hot chemical block region compared with the ambient mantle (Fig. 4d and e). This density contrast of $\Delta\rho'_{spin}$ provides an extra lifting force for the chemical layer which can raise the chemical material to the depth of ~ 1700 km with a flat top. This mechanism well explains the steep side boundaries and high elevations up to 1700 km depth for the Africa LLSVP. Our model results show that the height of the LLSVPs is dependent on their intrinsic chemical density contrasts in the internal heating cases. Though the height of LLSVP beneath the Pacific Ocean is still controversial (He and Wen, 2009; Tanaka et al., 2009), our results suggest that the intrinsic density contrast of the LLSVPs beneath Africa and the Pacific Ocean may be different from each other.

Iron-spin transition of ferropericlase has been observed experimentally at lower mantle pressure since 2003 (Badro et al., 2003) and confirmed by succeeding high-pressure experimental and theoretical investigations (e.g. Lin et al., 2013). Because of smooth feature of the transition, the spin transition seems invisible at one-dimensional sound velocity profile (Masters, 2008), which raises the question whether spin transition can be observed on Earth. Wu and Wentzcovitch (2014) found that spin transition of ferropericlase will produce observable signatures at seismic tomography because the P wave of pyrolytic lower mantle under spin transition becomes temperature insensitive around the depth of ~ 1750 km. These signatures have been widely reported in previous seismic tomography studies such as the disruption of P wave image below some hot spots (Zhao, 2007), the global disruption of P wave structure (van der Hilst and Kárason, 1999) at ~ 1700 km depth, anti-correlation between shear velocity and bulk sound velocity around middle lower mantle (Simmons et al., 2010), and discrepancy between P and S wave model at the origin depth of thermal plumes (Boschi et al., 2007). Here we further found that iron-spin transition may control the formation of LLSVPs, a signature of the spin transition from geodynamic aspect.

Most of the chemical blocks in our model last for about 200–300 Myr which is different from the studies of Burke et al. (2008) who suggested that the LLSVPs can survive beyond 300 Myr or much longer. In our model, the chemical materials mix with the ambient mantle after being stable for 200–300 Myr, suggesting that the LLSVPs can only survive in certain era of the evolution of the Earth. The chemical layer in the lower mantle may be formed from remnant of original chemical composition or the subducting slabs or the differentiation of materials at CMB. If they are made of recycled slabs, when new chemical materials are supplied from subduction, the LLSVPs may emerge periodically in the lower mantle. This process deserves more detailed studies in future work. We ignore the possible variation of viscosity caused by iron-spin transition because the experimental results are still obscure (Wentzcovitch et al., 2009). The effects of spin transition on viscosity may not be as significant as density distribution in shap-

ing the morphology of chemical blocks. Nevertheless, it may play an important role in the surviving time of blocks.

In summary, we include the effects of iron-spin transition of ferroperricite in thermochemical mantle convection model. This transition in spin state of iron helps the formation of large chemical blocks with steep side boundaries and high elevations to ~1200 km above the CMB. The similarity in geometry and shear velocity perturbation between the modeled chemical structures and the observed LLSVPs supports that iron-spin transition controls the formation of LLSVPs. The signatures of the iron-spin transition have also been shown widely at seismic tomography studies as suggested by Wu and Wentzcovitch (2014). The typical survival time of these blocks is 200–300 Myr, suggesting that the LLSVPs may be transient structures which can form in the lower mantle and can be destroyed by large scale mantle motion.

Acknowledgements

The authors thank Jung-fu Lin and Fan-chi Lin for their constructive suggestions. This study is supported by State Key Development Program of Basic Research of China (2014CB845905) and National Natural Science Foundation of China (41422402, 41274087 and 41374102). Wei Leng is also partially supported by the Fundamental Research Funds for the Central Universities (WK2080000053).

Appendix A. Supplementary material

Supplementary material related to this article can be found online at <http://dx.doi.org/10.1016/j.epsl.2015.05.006>.

References

- Badro, J., Fiquet, G., Guyot, F., Rueff, J.-P., Struzhkin, V.V., Vankó, G., Monaco, G., 2003. Iron partitioning in Earth's mantle: toward a deep lower mantle discontinuity. *Science* 300, 789–791.
- Bengtson, A., Li, J., Morgan, D., 2009. Mössbauer modeling to interpret the spin state of iron in (Mg,Fe)SiO₃ perovskite. *Geophys. Res. Lett.* 36. <http://dx.doi.org/10.1029/2009GL038340>.
- Boschi, L., Becker, T., Steinberger, B., 2007. Mantle plumes: dynamic models and seismic images. *Geochem. Geophys. Geosyst.* 8. <http://dx.doi.org/10.1029/2007GC001733>.
- Bower, D.J., Gurnis, M., Jackson, J.M., Sturhahn, W., 2009. Enhanced convection and fast plumes in the lower mantle induced by the spin transition in ferroperricite. *Geophys. Res. Lett.* 36. <http://dx.doi.org/10.1029/2009GL037706>.
- Burke, K., Steinberger, B., Torsvik, T.H., Smethurst, M.A., 2008. Plume generation zones at the margins of large low shear velocity provinces on the core–mantle boundary. *Earth Planet. Sci. Lett.* 265, 49–60.
- Christensen, U.R., Hofmann, A.W., 1994. Segregation of subducted oceanic crust in the convecting mantle. *J. Geophys. Res., Solid Earth* 99, 19867–19884.
- Deschamps, F., Trampert, J., 2003. Mantle tomography and its relation to temperature and composition. *Phys. Earth Planet. Inter.* 140, 277–291.
- Fujino, K., Nishio-Hamane, D., Seto, Y., Sata, N., Nagai, T., Shinmei, T., Irifune, T., Ishii, H., Hiraoka, N., Cai, Y.Q., 2012. Spin transition of ferric iron in Al-bearing Mg-perovskite up to 200 GPa and its implication for the lower mantle. *Earth Planet. Sci. Lett.* 317, 407–412.
- Glazyrin, K., Ballaran, T.B., Frost, D., McCammon, C., Kantor, A., Merlini, M., Hanfland, M., Dubrovinsky, L., 2014. Magnesium silicate perovskite and effect of iron oxidation state on its bulk sound velocity at the conditions of the lower mantle. *Earth Planet. Sci. Lett.* 393, 182–186.
- Grand, S.P., van der Hilst, R.D., Widiyantoro, S., 1997. Global seismic tomography: a snapshot of convection in the Earth. *GSA Today* 7, 1–7.
- Hansen, U., Yuen, D.A., 2000. Extended-Boussinesq thermal–chemical convection with moving heat sources and variable viscosity. *Earth Planet. Sci. Lett.* 176, 401–411.
- He, Y., Wen, L., 2009. Structural features and shear-velocity structure of the “Pacific Anomaly”. *J. Geophys. Res., Solid Earth* 114. <http://dx.doi.org/10.1029/2008JB005814>.
- Hsu, H., Blaha, P., Cococcioni, M., Wentzcovitch, R.M., 2011. Spin-state crossover and hyperfine interactions of ferric iron in MgSiO₃ perovskite. *Phys. Rev. Lett.* 106. <http://dx.doi.org/10.1103/PhysRevLett.106.118501>.
- Ishii, M., Tromp, J., 2004. Constraining large-scale mantle heterogeneity using mantle and inner-core sensitive normal modes. *Phys. Earth Planet. Inter.* 146, 113–124.
- Jarvis, G.T., Mckenzie, D.P., 1980. Convection in a compressible fluid with infinite Prandtl number. *J. Fluid Mech.* 96, 515–583.
- King, S.D., Lee, C., Van Keken, P.E., Leng, W., Zhong, S., Tan, E., Tosi, N., Kameyama, M.C., 2010. A community benchmark for 2-D Cartesian compressible convection in the Earth's mantle. *Geophys. J. Int.* 180, 73–87.
- Labrosse, S., Hernlund, J.W., Coltice, N., 2007. A crystallizing dense magma ocean at the base of the Earth's mantle. *Nature* 450, 866–869.
- Leng, W., Zhong, S., 2008. Controls on plume heat flux and plume excess temperature. *J. Geophys. Res., Solid Earth* 113. <http://dx.doi.org/10.1029/2007JB005155>.
- Lin, J.F., Watson, H., Vankó, G., Alp, E.E., Prakapenka, V.B., Dera, P., Struzhkin, V.V., Kubo, A., Zhao, J., McCammon, C., 2008. Intermediate-spin ferrous iron in low-temperature mantle post-perovskite and perovskite. *Nat. Geosci.* 1, 688–691.
- Lin, J.F., Speziale, S., Mao, Z., Marquardt, H., 2013. Effects of the electronic spin transitions of iron in lower mantle minerals: implications for deep mantle geophysics and geochemistry. *Rev. Geophys.* 51, 244–275.
- Lundin, S., Catalli, K., Santillán, J., Shim, S.H., Prakapenka, V.B., Kunz, M., Meng, Y., 2008. Effect of Fe on the equation of state of mantle silicate perovskite over 1 Mbar. *Phys. Earth Planet. Inter.* 168, 97–102.
- Marquardt, H., Speziale, S., Reichmann, H.J., Frost, D.J., Schilling, F.R., Garnero, E.J., 2009. Elastic shear anisotropy of ferroperricite in Earth's lower mantle. *Science* 324, 224–226.
- Masters, G., 2008. On the possible (1D) seismological signature of the spin crossover in ferroperricite. *AGU Fall Meet. Abstr.* 1, 04.
- McCammon, C., Kantor, I., Narygina, O., Rouquette, J., Ponkratz, U., Sergueev, I., Mezouar, M., Prakapenka, V., Dubrovinsky, L., 2008. Stable intermediate-spin ferrous iron in lower-mantle perovskite. *Nat. Geosci.* 1, 684–687.
- McNamara, A.K., Zhong, S., 2005. Thermochemical structures beneath Africa and the Pacific Ocean. *Nature* 437, 1136–1139.
- Moresi, L.N., Solomatov, V.S., 1995. Numerical investigation of 2D convection with extremely large viscosity variations. *Phys. Fluids* 7, 2154–2162.
- Ni, S., Tan, E., Gurnis, M., Helmberger, D., 2002. Sharp sides to the African superplume. *Science* 296, 1850–1852.
- Ni, S., Helmberger, D.V., 2003. Seismological constraints on the South African superplume; could be the oldest distinct structure on Earth. *Earth Planet. Sci. Lett.* 206, 119–131.
- Poirier, J.P., 2000. *Introduction to the Physics of the Earth's Interior*. Cambridge University Press, pp. 8–9.
- Ritsema, J., van Heijst, H.J., Woodhouse, J.H., 1999. Complex shear wave velocity structure imaged beneath Africa and Iceland. *Science* 286, 1925–1928.
- Shahnas, M.H., Peltier, W.R., Wu, Z., Wentzcovitch, R., 2011. The high-pressure electronic spin transition in iron: potential impacts upon mantle mixing. *J. Geophys. Res., Solid Earth* 116. <http://dx.doi.org/10.1029/2010JB007965>.
- Simmons, N.A., Forte, A.M., Boschi, L., Grand, S.P., 2010. GypSuM: a joint tomographic model of mantle density and seismic wave speeds. *J. Geophys. Res., Solid Earth* 115. <http://dx.doi.org/10.1029/2010JB007631>.
- Stackhouse, S., Brodholt, J.P., Price, G.D., 2007. Electronic spin transitions in iron-bearing MgSiO₃ perovskite. *Earth Planet. Sci. Lett.* 253, 282–290.
- Tackley, P.J., King, S.D., 2003. Testing the tracer ratio method for modeling active compositional fields in mantle convection simulations. *Geochem. Geophys. Geosyst.* 4. <http://dx.doi.org/10.1029/2001GC000214>.
- Tan, E., Gurnis, M., 2005. Metastable superplumes and mantle compressibility. *Geophys. Res. Lett.* 32. <http://dx.doi.org/10.1029/2005GL024190>.
- Tan, E., Gurnis, M., 2007. Compressible thermochemical convection and application to lower mantle structures. *J. Geophys. Res., Solid Earth* 112. <http://dx.doi.org/10.1029/2006JB004505>.
- Tan, E., Leng, W., Zhong, S., Gurnis, M., 2011. On the location of plumes and lateral movement of thermochemical structures with high bulk modulus in the 3-D compressible mantle. *Geochem. Geophys. Geosyst.* 12. <http://dx.doi.org/10.1029/2011GC003665>.
- Tanaka, S., Suetsugu, D., Shiobara, H., Sugioka, H., Kanazawa, T., Fukao, Y., Barruol, G., Reymond, D., 2009. On the vertical extent of the large low shear velocity province beneath the South Pacific Superswell. *Geophys. Res. Lett.* 36. <http://dx.doi.org/10.1029/2009GL037568>.
- Torsvik, T.H., Smethurst, M.A., Burke, K., Steinberger, B., 2008. Long term stability in deep mantle structure: evidence from the ~300 Ma Skagerrak-Centered Large Igneous Province (the SCLIP). *Earth Planet. Sci. Lett.* 267, 444–452.
- Tschauner, O., Ma, C., Beckett, J.R., Prescher, C., Prakapenka, V.B., Rossman, G.R., 2014. Discovery of bridgmanite, the most abundant mineral in Earth, in a shocked meteorite. *Science* 346, 1100–1102.
- van der Hilst, R.D., Káráson, H., 1999. Compositional heterogeneity in the bottom 1000 kilometers of Earth's mantle: toward a hybrid convection model. *Science* 283, 1885–1888.
- Wang, Y., Wen, L., 2007. Geometry and P and S velocity structure of the “African Anomaly”. *J. Geophys. Res., Solid Earth* 112. <http://dx.doi.org/10.1029/2006JB004483>.
- Wentzcovitch, R.M., Justo, J.F., Wu, Z., da Silva, C.R.S., Yuen, D.A., Kohlstedt, D., 2009. Anomalous compressibility of ferroperricite throughout the iron spin cross-over. *Proc. Natl. Acad. Sci.* 106, 8447–8452.
- Wentzcovitch, R.M., Yu, Y.G., Wu, Z., 2010. Thermodynamic properties and phase relations in mantle minerals investigated by first principles quasiharmonic theory. *Rev. Mineral. Geochem.* 71, 59–98.

- Wu, Z., Justo, J.F., da Silva, C.R.S., de Gironcoli, S., Wentzcovitch, R.M., 2009. Anomalous thermodynamic properties in ferropericlyase throughout its spin crossover. *Phys. Rev. B* 80. <http://dx.doi.org/10.1103/PhysRevB.80.014409>.
- Wu, Z., Justo, J.F., Wentzcovitch, R.M., 2013. Elastic anomalies in a spin-crossover system: ferropericlyase at lower mantle conditions. *Phys. Rev. Lett.* 110. <http://dx.doi.org/10.1103/PhysRevLett.110.228501>.
- Wu, Z., Wentzcovitch, R.M., 2014. Spin crossover in ferropericlyase and velocity heterogeneities in the lower mantle. *Proc. Natl. Acad. Sci.* 111, 10468–10472.
- Zhang, N., Zhong, S., Leng, W., Li, Z.X., 2010. A model for the evolution of the Earth's mantle structure since the Early Paleozoic. *J. Geophys. Res., Solid Earth* 115. <http://dx.doi.org/10.1029/2009JB006896>.
- Zhao, D., 2007. Seismic images under 60 hotspots: search for mantle plumes. *Gondwana Res.* 12, 335–355.
- Zhong, S., 2006. Constraints on thermochemical convection of the mantle from plume heat flux, plume excess temperature, and upper mantle temperature. *J. Geophys. Res., Solid Earth* 111. <http://dx.doi.org/10.1029/2005JB003972>.